

## Evidence of a recent magma dike intrusion at the slow spreading Lucky Strike segment, Mid-Atlantic Ridge

Robert P. Dziak,<sup>1</sup> Deborah K. Smith,<sup>2</sup> DelWayne R. Bohnenstiehl,<sup>3</sup> Christopher G. Fox,<sup>4</sup> Daniel Desbruyeres,<sup>5</sup> Haru Matsumoto,<sup>1</sup> Maya Tolstoy,<sup>3</sup> and Daniel J. Fornari<sup>2</sup>

Received 15 April 2004; revised 2 September 2004; accepted 30 September 2004; published 4 December 2004.

[1] Mid-ocean ridge volcanic activity is the fundamental process for creation of ocean crust, yet the dynamics of magma emplacement along the slow spreading Mid-Atlantic Ridge (MAR) are largely unknown. We present acoustical, seismological, and biological evidence of a magmatic dike intrusion at the Lucky Strike segment, the first detected from the deeper sections (>1500 m) of the MAR. The dike caused the largest teleseismic earthquake swarm recorded at Lucky Strike in >20 years of seismic monitoring, and one of the largest ever recorded on the northern MAR. Hydrophone records indicate that the rate of earthquake activity decays in a nontectonic manner and that the onset of the swarm was accompanied by 30 min of broadband (>3 Hz) intrusion tremor, suggesting a volcanic origin. Two submersible investigations of high-temperature vents located at the summit of Lucky Strike Seamount 3 months and 1 year after the swarm showed a significant increase in microbial activity and diffuse venting. This magmatic episode may represent one form of volcanism along the MAR, where highly focused pockets of magma are intruded sporadically into the shallow ocean crust beneath long-lived, discrete volcanic structures recharging preexisting seafloor hydrothermal vents and ecosystems.

**INDEX TERMS:** 3035 Marine Geology and Geophysics: Midocean ridge processes; 7280 Seismology: Volcano seismology (8419); 8149 Tectonophysics: Planetary tectonics (5475); 4259 Oceanography: General: Ocean acoustics; 9325 Information Related to Geographic Region: Atlantic Ocean; **KEYWORDS:** Mid-Atlantic Ridge, earthquake, hydroacoustic

**Citation:** Dziak, R. P., D. K. Smith, D. R. Bohnenstiehl, C. G. Fox, D. Desbruyeres, H. Matsumoto, M. Tolstoy, and D. J. Fornari (2004), Evidence of a recent magma dike intrusion at the slow spreading Lucky Strike segment, Mid-Atlantic Ridge, *J. Geophys. Res.*, 109, B12102, doi:10.1029/2004JB003141.

### 1. Introduction

[2] Seafloor magmatic activity is the fundamental process for creation of new ocean crust and for the transfer of thermal energy from the mantle to the oceans leading to the creation of seafloor hydrothermal systems and chemosynthetic ecosystems [e.g., *Corliss et al.*, 1979; *Spiess et al.*, 1980; *East Pacific Rise Group*, 1981]. Yet seafloor volcanic activity rarely has been observed along the deep ocean (>1000 m) portions of the global mid-ocean ridge (MOR) system due to the extreme difficulty in performing continuous in situ monitoring of the seafloor and the inferred long

recurrence intervals (from decades to centuries) of MOR volcanic activity. The first detection of deep ocean MOR eruptions occurred in the Pacific through serendipitous observations of ocean thermal anomalies and recently erupted lava flows [*Baker et al.*, 1987; *Haymon et al.*, 1993]. To our knowledge, the only example of in situ observations of a seafloor eruption in progress occurred during the 1998 Axial Volcano (Juan de Fuca Ridge) eruption recorded by water temperature and seafloor deformation sensors deployed within the volcano's caldera. Development of cabled, deep ocean observatories with a variety of geophysical, chemical, and biological sensors offer the best opportunity to directly sample multiple aspects of seafloor eruptions as they occur. Although deployment of these types of systems is rapidly approaching, it will be several years before widespread, real time in situ monitoring is accomplished.

[3] Currently, the best method to observe deep ocean MOR volcanic activity in real time is by the remote detection of seismicity associated with the intrusion of magma through the brittle ocean crust. Global and regional seismic networks offer critical information on the spatial patterns and source mechanisms of seismicity in the ocean basins [*Blackman et al.*, 2000; *Tolstoy et al.*, 2001]. However, the low magnitude of earthquakes associated with

<sup>1</sup>Cooperative Institute for Marine Resource Center, Oregon State University/National Oceanic and Atmospheric Administration, Newport, Oregon, USA.

<sup>2</sup>Woods Hole Oceanographic Institution, Woods Hole, Massachusetts, USA.

<sup>3</sup>Lamont-Doherty Earth Observatory, Columbia University, Palisades, New York, USA.

<sup>4</sup>Pacific Marine Environmental Laboratory, NOAA, Newport, Oregon, USA.

<sup>5</sup>Departement Environnement Profond, Centre de Brest de IFREMER, Plouzane, France.

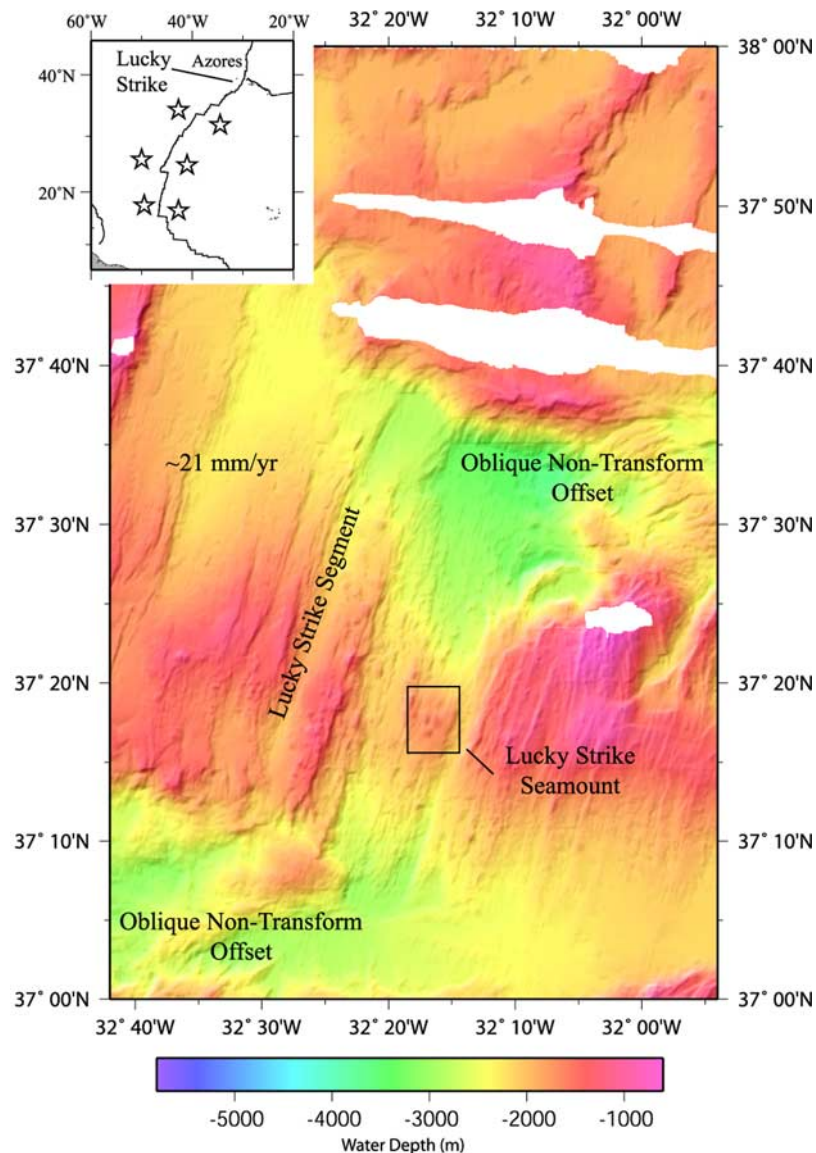


**Figure 1.** Bathymetric map of the slow spreading ( $21 \text{ mm yr}^{-1}$ ) Lucky Strike segment, Mid-Atlantic Ridge [after *Escartin et al.*, 2001]. Inset map shows location of the moored hydrophone array (stars) and Lucky Strike segment along the northern Mid-Atlantic Ridge. Box shows location of Figure 2. The Lucky Strike segment is magmatically robust compared to other MAR segments due to its proximity to the Azores hot spot.

MOR volcanic activity, at least at fast and medium spreading ridges [*Einarsson*, 1991; *Dziak et al.*, 1995], and the relatively high detection thresholds of land-based seismic networks ( $M > 4$ ) for the majority of the global MOR system, often results in an incomplete picture of the volcanic episode or a failure to detect the episode altogether. In situ ocean bottom seismometer experiments are able to detect the microseismicity associated with seafloor spreading, but only monitor small sections of the ridge for limited times. In the last decade with the release of the U.S. Navy hydrophone array data in the north Pacific ocean, hydroacoustic methods have been developed to monitor the hydroacoustic tertiary phase or  $T$  wave of MOR seismic activity [*Fox et al.*, 1994]. Since acoustic  $T$  waves propagating in the ocean sound channel obey cylindrical spreading ( $r^{-1}$ ) energy loss as opposed to the spherical spreading

( $r^{-2}$ ) of solid-earth seismic  $P$  waves, sound channel hydrophones can often detect smaller ( $M < 4$ ) and therefore more numerous earthquakes than land-based seismic networks [*Dziak et al.*, 2004].

[4] The use of hydroacoustic methods to detect MOR volcanic activity has met with success, allowing for the first real-time observation of a magma dike injection and seafloor eruption episode along the Juan de Fuca mid-ocean ridge [*Dziak et al.*, 1995; *Fox et al.*, 1995]. The remote detection of this volcanic episode resulted in several in situ multidisciplinary studies [*Baker et al.*, 1995; *Embley et al.*, 1995], leading to the first discovery of microbial communities living in a subseafloor ecosystem [*Juniper et al.*, 1995; *Holden et al.*, 1998]. Although remote detection of volcanic activity necessitates the coordination of research vessels to the MOR site in “response” to the volcanic event

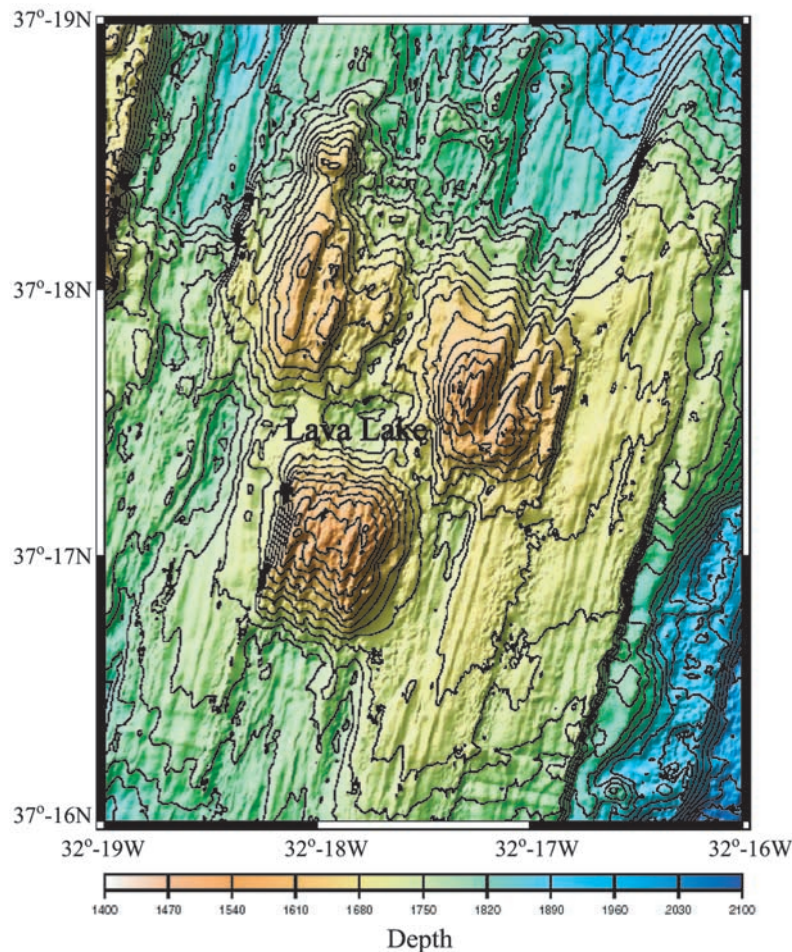


**Figure 2.** Detailed bathymetry of Lucky Strike Seamount. The 8 km wide, 1 km high seamount is composed of three main basalt cones, with a vigorous hydrothermal system and lava lake at its summit [after Scheirer *et al.*, 2000] (with kind permission of Springer Science and Business Media). Contour interval is 200 m.

[Cowen *et al.*, 2004], this remains the only currently available method for real-time detection and in situ confirmation of a MOR volcanic eruption.

[5] Since the U.S. Navy hydrophones are clearly of use in monitoring MOR volcanic activity but are placed at fixed locations on the seafloor, NOAA/Oregon State University developed an autonomous hydrophone that could be deployed anywhere in the global oceans [Fox *et al.*, 2001a]. A six-element array of these autonomous hydrophones has been moored within the ocean sound channel along the flanks of the Mid-Atlantic Ridge (MAR) between 15°–35°N since February 1999 [Smith *et al.*, 2002, 2003]. The hydrophones are used to estimate the acoustic location of earthquakes from throughout the Atlantic Ocean basin. For events within the array, hydrophones allow for a reduction in the magnitude of completeness from  $M_c = 4.7 m_b$  using the land-based seismic networks to  $M_c = 3.0 m_b$  [Dziak *et al.*, 2004]. The improved detection capability of the hydrophones allows for a better view of the overall spatiotemporal patterns of MAR earthquakes and the partitioning between magmatic and tectonic events at this slow spreading ridge [Smith *et al.*, 2002; Bohnenstiehl *et al.*, 2002, 2003; Escartin *et al.*, 2003]. As in the Pacific, it is

anticipated that hydroacoustic monitoring will provide insights into dike emplacement and eruption dynamics along the MAR. The hydrophones do not yet have real-time capability but are deployed and recovered on a yearly schedule. Earthquake locations are therefore available  $\sim 1.5$  years after the events occurred.

[6] The northern MAR is a classic slow spreading ridge with an average full spreading rate of  $\sim 25 \text{ mm yr}^{-1}$ . In general, the MAR is characterized by a 1.5–3 km deep, 15–30 km wide axial rift valley with major transform faults that offset the ridge along its length. The rift valley commonly contains an axial volcanic ridge that is considered to be the predominant site of volcanic activity [Ballard and van Andel, 1977]. On the basis of the sizes of the volcanic ridges, large volumes of lava must be erupted on the valley floor [Smith and Cann, 1993]. Currently, however, we do not know how frequently magmatic events occur, whether they migrate along the axis, whether there are spatial patterns in these events, or how they vary through time.

[7] During 16–17 March 2001 a swarm of 147 earthquakes occurred along the Lucky Strike segment of the MAR near 37°N (Figure 1). The Lucky Strike spreading segment is strongly influenced by its proximity to the

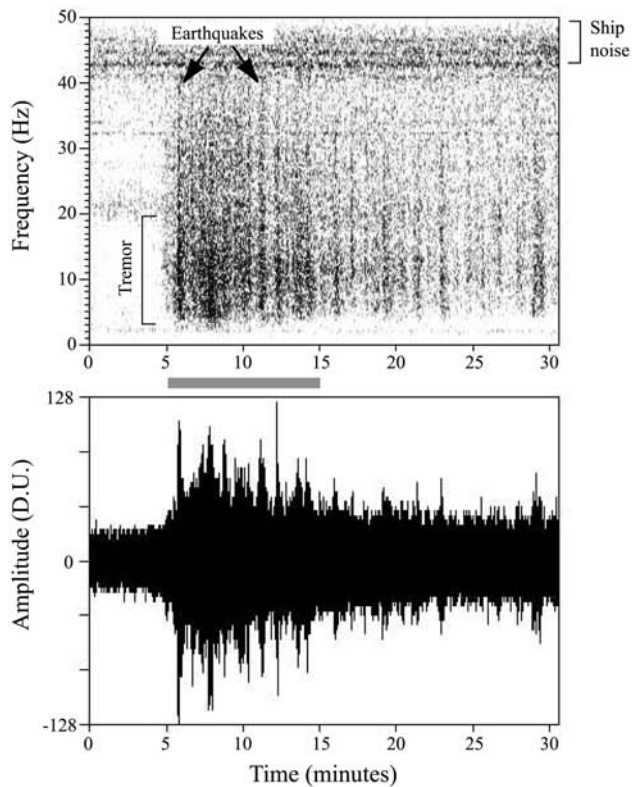


**Figure 3.** Time series and spectrogram of the northeast hydrophone (closest to the Lucky Strike segment) showing the onset of the 16 March 2001 earthquake swarm. (bottom) Vertical axes for the time series diagram shows amplitude in digital units; (top) spectrogram is in frequency (Hz). Broadband, impulsive earthquake arrivals stand out against a background of low-frequency (3–15 Hz) continuous tremor energy. Gray bar shows the section of the hydrophone signal highlighted in Figure 11.

Azores Hot spot, and it is magmatically robust compared to other segments of the MAR [Detrick *et al.*, 1995]. The segment is characterized by a broad rift valley (~12 km wide), and exhibits the greatest depth contrast, both across and along axis, of any segment on this part of the MAR [Scheirer *et al.*, 2000]. The center of the segment is dominated by the 8 km wide, 1 km high Lucky Strike Seamount (Figure 2). The seamount hosts a vigorous hydrothermal system and a lava lake [Humphris *et al.*, 2002]. The purpose of this study is to present evidence of a dike emplacement episode at the Lucky Strike segment, the first detected along a deep ocean portion of the MAR, and thereby provide insights into the dynamics of magmatic processes along slow spreading ridges.

## 2. Description of the Lucky Strike Earthquake Swarm

[8] The Lucky Strike earthquake swarm recorded on the hydrophone array (Figures 3–5) began on 16 March at 1528 UT and continued for ~29 hours. Nearly half of the 147 hydrophone-detected events occurred in the first 1.5 hours reaching a peak of 42 events per hour, but thereafter rapidly declined to 5 events per hour. The first

four earthquakes of the swarm occurred near Lucky Strike Seamount and were accompanied by 30 min of continuous, low-frequency, broadband energy (3–20 Hz) that was interpreted as volcanic tremor. Within minutes, however, the events began locating north of the volcano and within the Lucky Strike rift valley, giving the appearance that the entire segment was undergoing a seafloor spreading episode (Figures 5 and 6a). The acoustic earthquake locations displayed through time (Figure 6a) show that the earthquakes occurred along the ridge segment throughout the swarm's duration and showed no evidence of along axis migration as has been observed during dike emplacement episodes at intermediate or ultraslow spreading ridges [Dziak and Fox, 1999; Tolstoy *et al.*, 2001].

[9] The hydroacoustic earthquake source locations were estimated from the hydrophone data using an iterative nonlinear regression algorithm. The algorithm minimizes the error between observed and predicted travel time by incrementing an event's latitude, longitude, and origin time [Dziak *et al.*, 1995]. Travel times and velocities along  $T$  wave ray paths are estimated by applying propagation models to the U.S. Navy ocean sound speed model, the Generalized Digital Environmental Model [Davis *et al.*, 1986]. Accurate ocean sound speed models and good azimuthal distribution of the autonomous hydrophone array relative to the MAR allows for well-constrained earthquake locations. Event location error is available as output from the regression algorithm covariance matrix [Bevington and Robinson, 1992, Chapter 11], with the range in location error of  $\pm 0.2'$ – $16.2'$  in latitude and  $\pm 0.3'$ – $20.4'$  in longitude at the 68% confidence interval (Figure 5). Since the Lucky Strike segment is ~350–400 km outside (north) of the hydrophone array, the earthquake swarm locations are not optimally constrained. The peak amplitude of the center of the  $T$  wave envelope is typically selected as the arrival time of the earthquake for location purposes since it corresponds to the high-energy phases radiated from nearest the epicentral region [Slack *et al.*, 1999]. The highest amplitudes of the  $T$  wave also correspond to the broadest band arrivals of the signal packet, meaning these phases propagated closest to the axis of the sound channel. Propagation along the sound channel is the least attenuated path as well as the slowest, meaning the highest-amplitude phase arrives late in the coda and does not form the clear, high S/N first-motion arrival that narrow-band  $P$  wave arrivals will do on seismometers. The acoustic epicenter can be different from the seismic epicenter, however, since it simply reflects the point at which the earthquake generated acoustic phases enter the sound channel and may be influenced by seafloor roughness or local bathymetry [Dziak *et al.*, 1997].

[10] The U.S. National Earthquake Information Center (NEIC), using land-based seismometers, located 33 earthquakes ( $3.6 \leq m_b \leq 5.0$ ) from the Lucky Strike swarm (Figure 5; white triangles), the first occurring at 1530 UT on 16 March. NEIC locates three of the swarm earthquakes at Lucky Strike Seamount, roughly nine events within the Lucky Strike segment north of the seamount, and the rest are located either along an intraplate region west and north of the rift valley or well outside (north and south) of the rift valley all together. The largest earthquake ( $M_w = 5.0$ ; large triangle on Figure 5) has a normal fault Harvard CMT solution (nodal plane with strike  $38^\circ$ , dip  $56^\circ$ , rake  $-102^\circ$ )

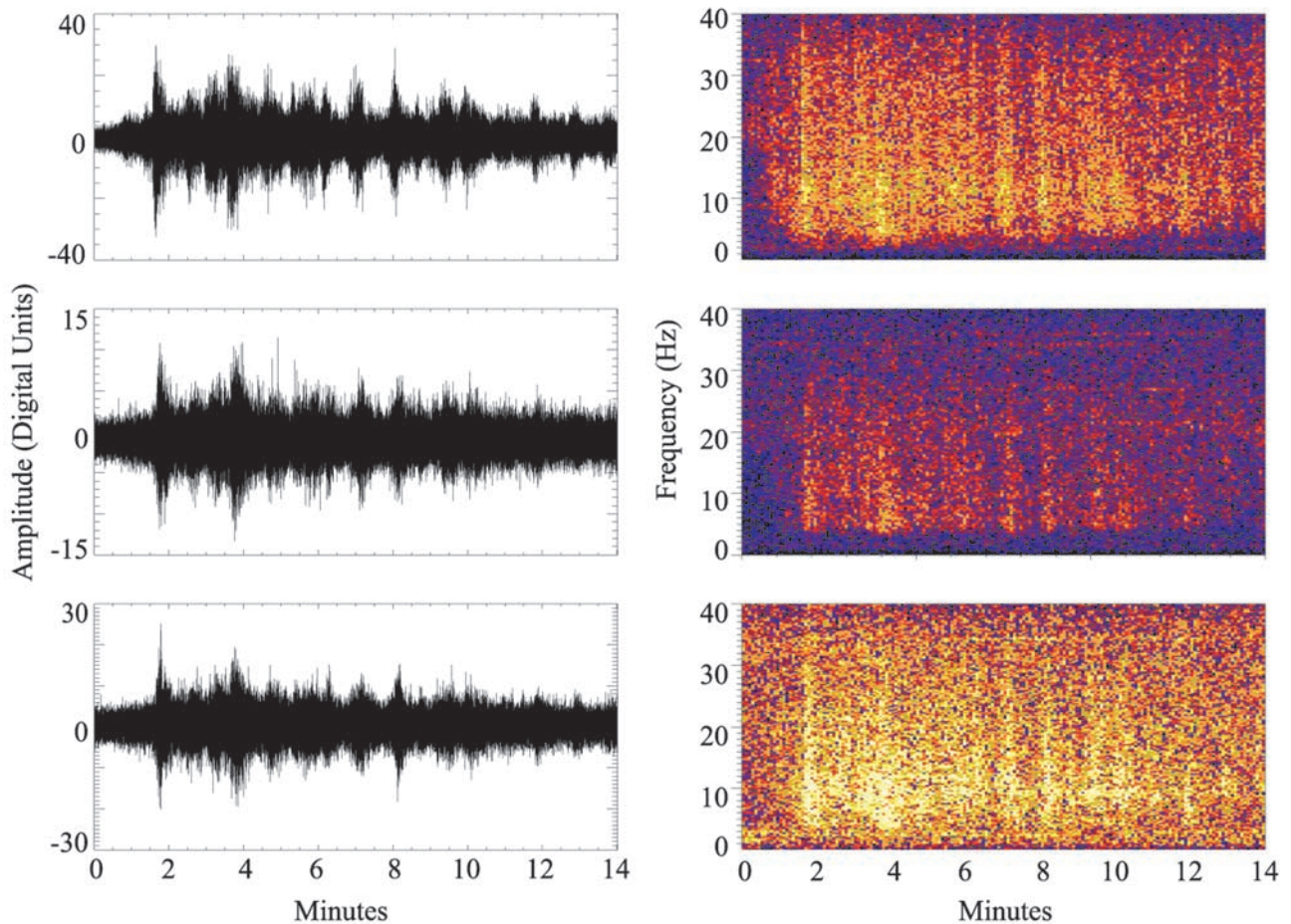


**Figure 4.** Example time series and spectrograms showing the onset of the Lucky Strike earthquake swarm recorded on three other hydrophones (northwest, center east, southeast hydrophones, top to bottom) to illustrate the  $T$  wave signal coherence across the array. In the spectrograms, yellow and red indicate relatively high acoustic energy, and blue indicates relatively low energy.

but occurred 5.5 hours into the swarm after the majority of the hydroacoustic seismicity (78 events) had occurred, supporting the preliminary interpretation this was not a typical main shock–aftershock sequence.

[11] The teleseismic locations of the Lucky Strike earthquakes differ by 8–100 km to the north-northwest of the hydroacoustically derived locations (Figure 7). Both seismic and hydroacoustic locations have biases; however, the acoustic locations are likely better constrained due to accurate ocean sound speed models available from years of oceanographic sampling and proximity of the hydrophones to the earthquake source [Smith *et al.*, 2002]. A recent study by Yang and Forsyth [2003] showed there is no systematic bias between  $T$  wave derived regional earthquake locations and locations derived from seismic surface waves, indicating the differences between locations may be due in part to the relative network geometry (acoustic versus seismic) or the variance of the bathymetry at the epicenter. The resultant vector differences between the hydroacoustically and teleseismically derived epicenters within the Lucky Strike segment are consistent with those found in a comparative study of 112 events within the array, 15–35°N [Bohnenstiehl and Tolstoy, 2003]. The majority of seismic stations monitoring the North Atlantic are located in North

America, most likely leading to a biasing of seismic locations to the north and west of the MAR. Biasing of the acoustic locations due to shallow bathymetry does not appear to be a significant factor here since hydrophone-detected earthquakes are in the deepest part of the Lucky Strike segment. Also, the earthquake acoustic locations are both on the north and south side of the bathymetric high of the segment, Lucky Strike Seamount. If the earthquake locations were being biased because of shallow bathymetry, then it might be expected that the acoustic earthquake locations would be biased toward the hydrophone array and locate along the south side of the seamount. This, however, is not the case.

[12] All depths of the teleseismic events were listed at 10 km. NEIC depths of 10 km represent fixed event depths, meaning that for these teleseismically located earthquakes there is generally little depth control. The risetime, or the time from the emergence of the  $T$  wave signal above ambient noise to the peak amplitude of a hydroacoustic envelope, has been shown to be a proxy for the relative depths of earthquakes [Schreiner *et al.*, 1995; Yang and Forsyth, 2003]. A decrease in risetimes has been interpreted to reflect shoaling of a dike as it propagated along a rift zone [Schreiner *et al.*, 1995; Dziak and Fox, 1999], with

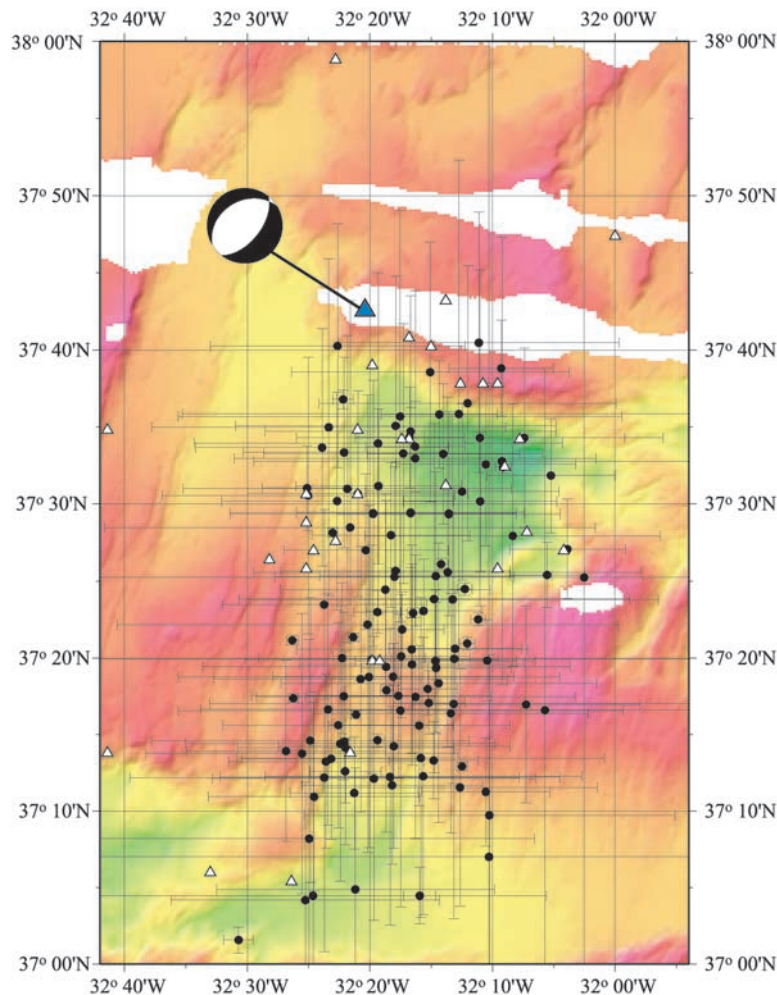


**Figure 5.** Hydroacoustic and teleseismic locations of the 16–17 March 2001 earthquake swarm at Lucky Strike segment. Black circles show hydroacoustic earthquake locations (147 events; error bars =  $1\sigma$ ), and white triangles show teleseismic locations (33 events). Blue triangle shows teleseismic location of largest event detected ( $M_w = 5.0$ ) during the swarm, moment tensor solution from the Harvard catalog (available from the U.S. Geological Survey, National Earthquake Information Center, online earthquake catalog, 2003, available at <http://neic.usgs.gov/neis/epic/epic.html>), and compressional quadrants are shaded.

spatiotemporal clustering of earthquakes with very short risetimes ( $<2$  s) representing actual magma eruption onto the seafloor. *Yang and Forsyth* [2003] modeled risetime changes and showed for focal depths of 1, 3, and 6 km that the  $T$  wave packet's risetimes will increase by several seconds with increasing earthquake depth. The risetimes of the Lucky Strike earthquake swarm (Figure 6b) are very short ( $<5$ – $10$  s) during the initial 5 hours of the swarm and then substantially increased afterward. The largest observed  $T$  wave risetime (47 s) corresponds to the  $M_w = 5.0$  teleseismic earthquake that occurred 5.5 hours after the beginning of the swarm. Although the risetime values are more or less evenly distributed along the entire Lucky Strike segment, Figure 6c does show the shortest risetimes and the smallest maximum risetime values clustered at Lucky Strike Seamount. Interpretation of the risetime information suggests the Lucky Strike earthquakes were shallowest at the onset of the swarm, and at and near Lucky Strike

Seamount, then deepened through time and at the distal ends of the segment. The risetime analysis will be summarized further in section 7.

[13] Long- and short-term histograms of acoustic and teleseismic events from the Lucky Strike segment are shown in Figures 8a and 8b. The majority of hydrophone earthquakes occurred within the first 5 hours of the Lucky Strike swarm, with the majority of the large teleseismic events occurring afterward. Given the hydrophones have a lower detection threshold than the teleseismic networks, this implies the low-magnitude ( $m_b \leq 3.5$ ) earthquakes detected only on the hydrophones occurred at the beginning of the swarm and became larger through time. This is consistent with an initial intrusion of magma into the shallow crust, followed by segment-scale normal faulting response to the stress perturbation induced by the magmatic intrusion. The histogram of the long-term seismicity from the Lucky Strike segment shows that the 16–17 March 2001 swarm was the

largest recorded at the Lucky Strike segment in 20+ years of seismic monitoring. From the time the hydrophones were first deployed in February 1999 until the start of the March 2001 swarm, a total of eleven earthquakes occurred at Lucky Strike with at most two earthquakes occurring on any single day. The last earthquakes recorded on the hydrophones before the March 2001 swarm were two events on 21 December 2000, thus providing little precursory information that a large swarm was imminent.

### 3. Magnitude-Time Distribution and Seismic Event Rate

[14] Other methods [Mogi, 1963; Sykes, 1970] to assess the relative magmatic/tectonic components of an earthquake

swarm are through analysis of the distribution of earthquake magnitudes through time as well as the frequency of occurrence of the largest events and the rate of decline of the seismic activity. Figure 9 shows the time-magnitude history of Lucky Strike earthquakes during the March 2001 sequence using acoustic source level (SL) versus time for events located using the hydrophone array (Figure 9a), and body wave magnitude ( $m_b$ ) versus time for events in the NEIC catalog (Figure 9b). The sequence lacks a dominant main shock earthquake typical of a tectonic earthquake sequence. Figure 10 shows the cumulative number of earthquakes as a function of time for both the full catalog of locatable hydrophone earthquakes and the subset with source levels (SLs)  $\geq 210$  dB. During tectonic sequences, large magnitude earthquakes are typically followed by a sequence of smaller magnitude events (aftershocks), with an event rate that decays as  $\sim 1/t^p$  (Omori's law), which reflects the relaxation of stress within the lithosphere. In Figure 10, synthetic Omori's law curves are shown for a  $p$  value of 1.1, the global median value [Utsu *et al.*, 1995] and a higher  $p$  value of 1.57 as observed for a normal faulting sequence near 24.5°N on the MAR [Bohnenstiehl *et al.*, 2002]. These decay curves do not describe the observed Lucky Strike distribution well relative to known aftershock sequences [cf. Bohnenstiehl *et al.*, 2002]. There is an abrupt decrease in the rate of activity near 0.05 days, with near constant event rates before and after this break. Such behavior is inconsistent with aftershock activity and suggests a magmatic component to the Lucky Strike earthquake swarm. Although somewhat larger spatial and temporal scales were involved, near-uniform and abruptly changing event rates have been noted seismically in association with a probable volcanic swarm along the ultraslow spreading Gakkel Ridge in 1999 [Tolstoy *et al.*, 2001].

### 4. Evidence of Volcanic Tremor

[15] A broadband, continuous tremor-like energy accompanied the onset of the Lucky Strike earthquake swarm. Intrusion tremor observed at Krafla Volcano in Iceland is very similar to the tremor observed here, with a broad

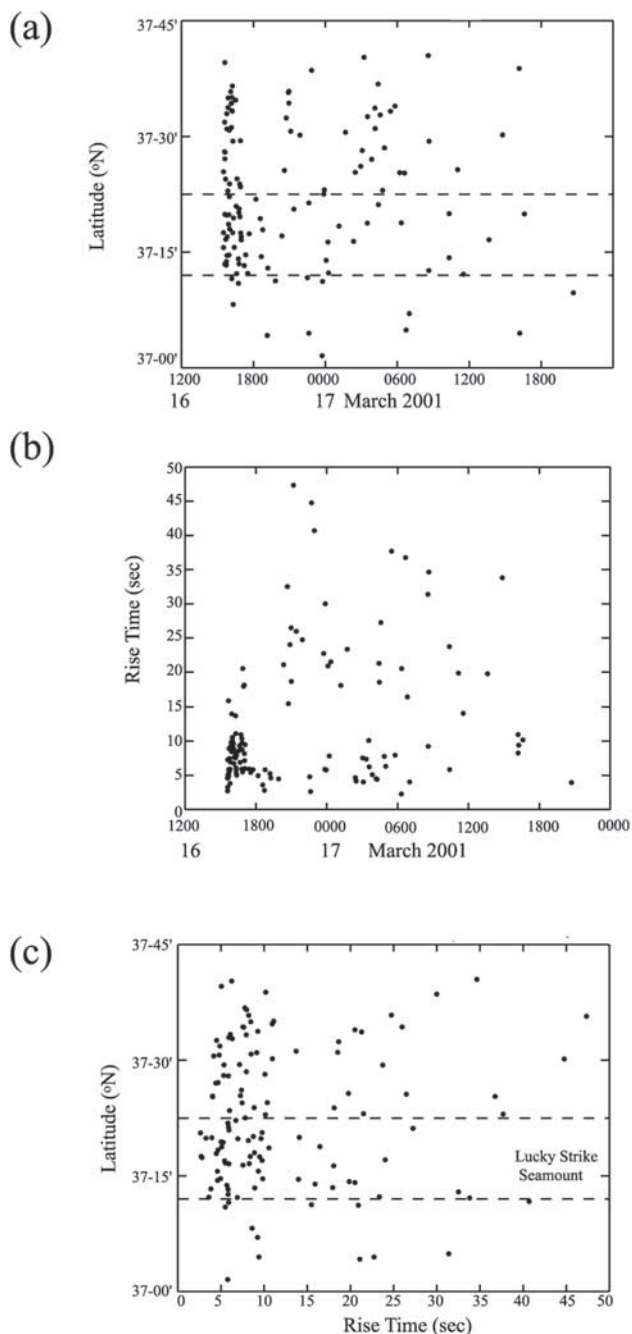


**Figure 6.** Time-distance and risetime diagrams of the Lucky Strike earthquake swarm estimated from the hydrophone records. (a) A time latitude of the Lucky Strike swarm. Dashed lines show north-south limit of Lucky Strike Seamount. The earthquakes appear to have occurred simultaneously along the entire  $\sim 50$  km length of the segment. There also is no clear evidence of migration of epicenters along the ridge axis, as has been shown to occur during lateral magma dike injection/eruptions observed on intermediate and ultraslow spreading ridges. (b) Earthquakes with the shortest risetimes that occurred at the onset and first 3 hours of the earthquake swarm suggesting that the earthquakes began shallow and deepened during the swarm. (c) Shortest risetimes and the smallest maximum risetime values of the entire segment that appear to cluster at Lucky Strike Seamount. Clustering of short risetime earthquakes ( $< 2$  s) has been correlated to MOR seafloor eruption sites [Dziak and Fox, 1999].

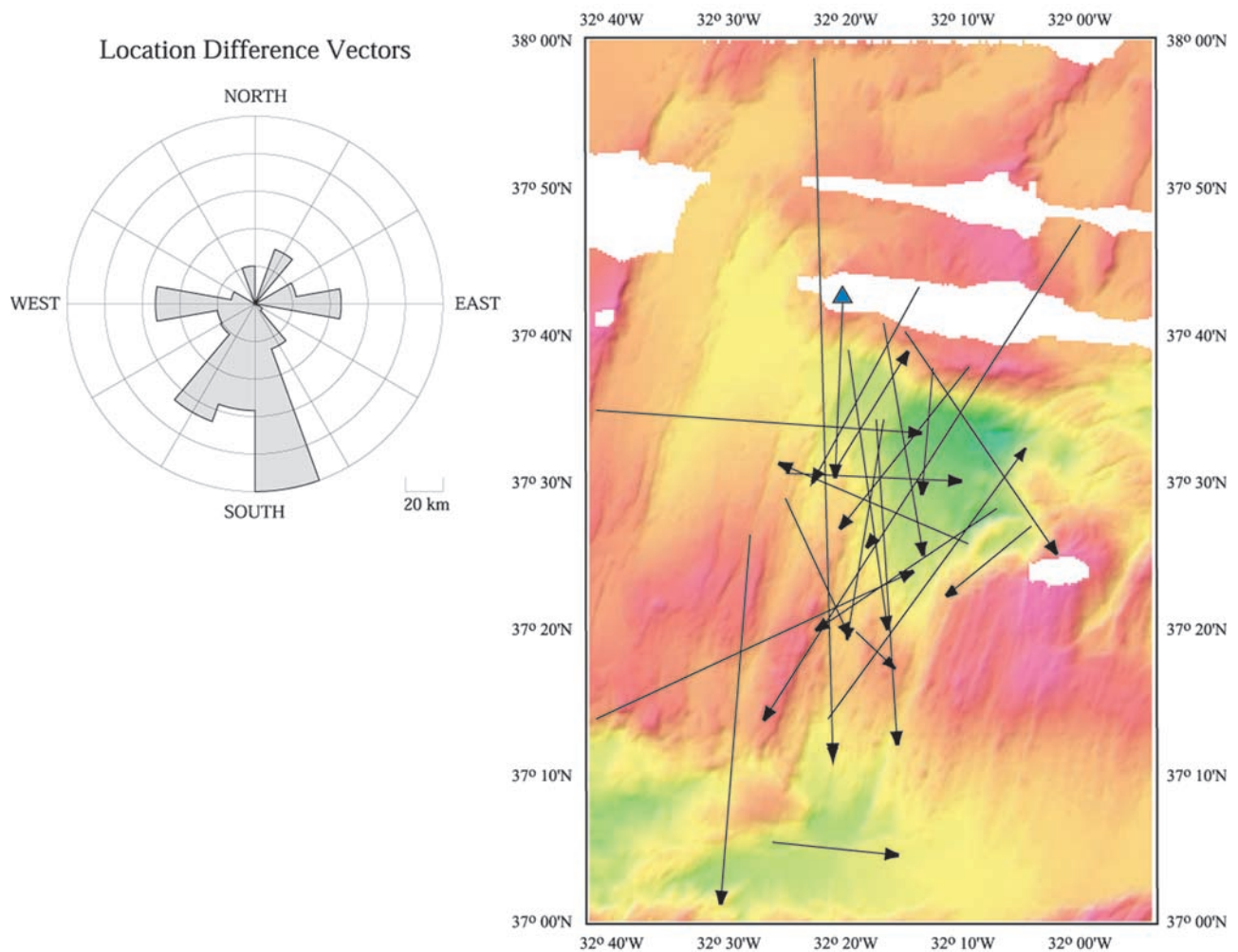


**Figure 7.** Diagrams of the location difference vectors between the teleseismic and hydroacoustically derived Lucky Strike earthquake epicenters (left) as rose plot and (right) in map view. The acoustic earthquake locations are 8–100 km to the south-southeast of the teleseismic locations and in general locate more within the segment valley than the teleseismic locations. Bathymetric steering does not seem to be a significant factor since many of the hydroacoustic earthquake locations are within the deepest portions of the ridge segment.

spectrum and predominant frequencies  $>3$  Hz [Brandsdottir and Einarsson, 1992]. Intrusions of small magma dikes at Krafla generally are accompanied by tremor mixed with swarms of small earthquakes. Intrusion tremor and earthquakes usually stop when the magma reaches the surface and the dike stops propagating. There is clear broadband energy present on the hydrophones from 3 Hz up to at least 30 Hz (Figures 11 and 12). The hydrophone response curves are flat from 10 to 55 Hz but decline  $\sim 20$  dB from 10 Hz down to 1 Hz, indicating this energy is strong enough to be detected even through the limitations of the instrument response. The question is, however, whether the source of this broadband energy is acoustic reverberation in the water column from the large amount of seismicity, or is the energy the result of cracking of the shallow ocean crust from the intrusion of magma. The first step is to prove that the “tremor” energy is significant. Figure 11 shows the spectrogram (dB power as a function of time) of the onset of Lucky Strike earthquake swarm, and illustrates the large

interearthquake energy. The record is from the northeast hydrophone, which has the smallest epicentral distance to the Lucky Strike segment. The numbers on the spectrogram show the location of the relative power calculations, with the frequency range and time duration of the power estimates shown in the adjacent table. The 1–30 Hz band was chosen since the hydrophone band-pass filter begins at 1 Hz and the tremor energy appears present up to 30 Hz. The overall lack of power under 3 Hz may be a result of filtering, in a sense, imposed on the signal by the physical width of the ocean sound channel ( $\sim 500$  m in cross-sectional depth). These power level estimates demonstrate there are significant acoustic signals between earthquake phases (2, 3, 4, and 5) at the onset of the swarm that is well above ambient noise levels (1 and 6).

[16] Second, it would be expected that earthquake and tremor signals should have dominant energies in different frequency bands. Figure 12 shows the detailed spectra of an earthquake, volcanic tremor, and ambient noise from the



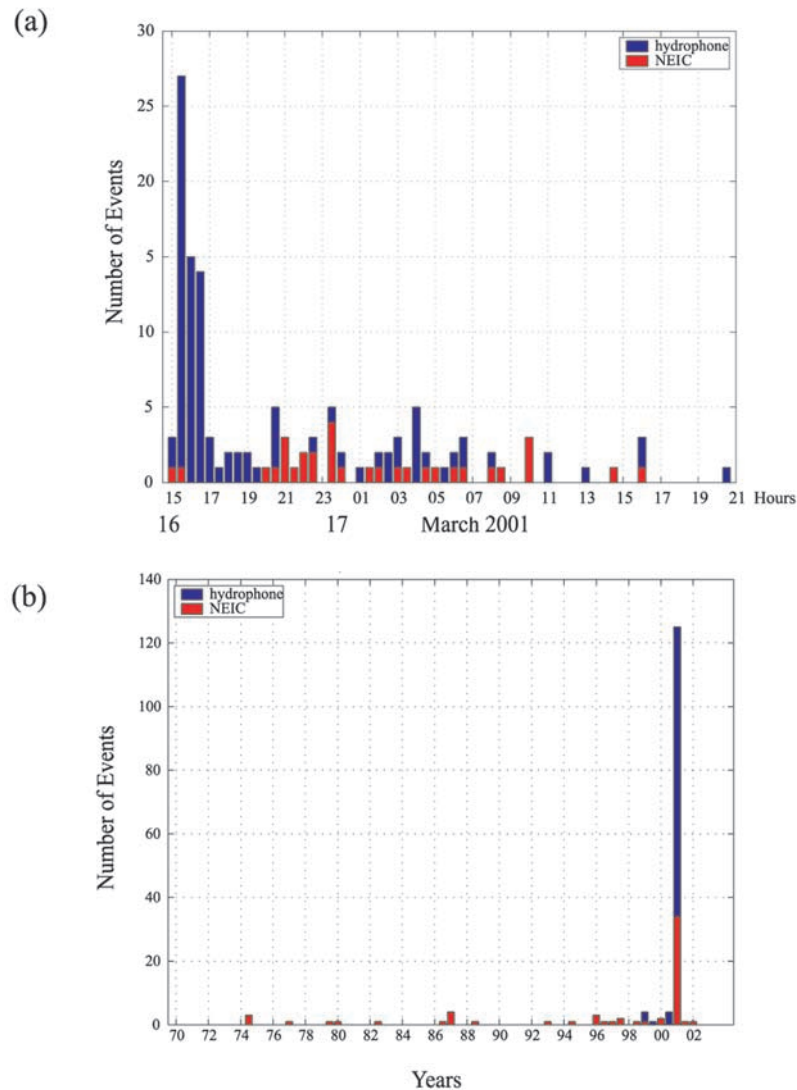


**Figure 8.** (a) Histogram of the Lucky Strike earthquake swarm showing both hydroacoustic and teleseismic (NEIC) earthquake counts. Bars show number of earthquakes in 30-min increments. (b) Histogram of the long-term seismicity located at the Lucky Strike segment. Number of events is in 6-month increments. The 16–17 March 2001 swarm was the largest recorded at the Lucky Strike segment in >20 years of seismic monitoring.

northeast hydrophone during the onset of the Lucky Strike swarm. The ambient noise spectra were calculated by taking a 66.6 s duration window of time series data  $\sim 1$  min before the first earthquake of the swarm. If the tremor signal is a result of magma injecting through the crust and not simply reverberation (reflection/refraction) of earthquake acoustic signals in the water column, then it should have a different frequency content than the earthquakes. The tremor and earthquake have different dominant frequencies, although their overall bandwidth appears to be the same (ship noise dominates the >42 Hz range). The tremor and earthquake relative amplitudes also have distinctly different levels. Since volcanic tremor normally has much lower source energy than earthquakes [Chouet, 1992], this does not help address the question of the tremor's source. Also, if the energy is from reverberation, the amplitude should also be

lower due to signal attenuation. This line of reasoning is therefore inconclusive. The timing of the tremor is, however, significant in that it occurs at the very beginning of the earthquake swarm and is not observed at any other time. Thus the evidence provided here indicates the interearthquake energy is significant, and although may in part be due to reverberation of the earthquake acoustic signals through the water column, the occurrence of this energy at the swarm's onset only and its similarity to tremor observed at subaerial volcanic systems argues for a magmatic origin.

## 5. In Situ Observations

[17] Previously documented mid-ocean ridge eruptions provided an abundance of seafloor and water column

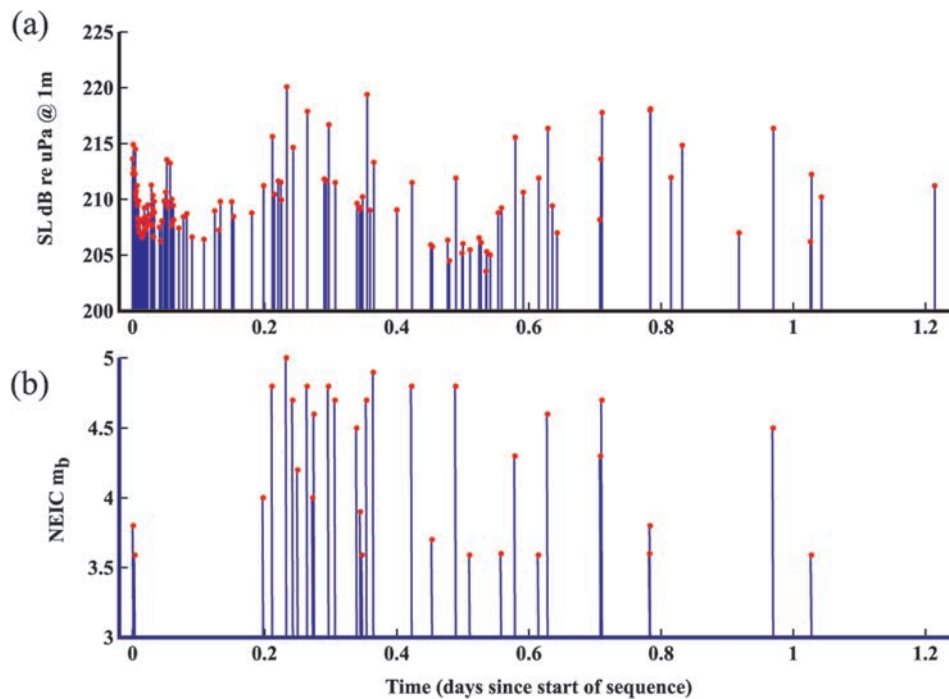


**Figure 9.** Time-magnitude history of Lucky Strike earthquakes during the 2001 sequence. (a) Acoustic source level (SL) versus time for events located using the AUH array. (b) Body wave magnitude ( $m_b$ ) versus time for events in the NEIC catalog. The sequence lacks a dominant main shock earthquake.

evidence allowing for confirmation of magmatic activity [e.g., Baker *et al.*, 1999; Embley *et al.*, 1999]. In situ observations of the high-temperature hydrothermal systems on the summit of Lucky Strike Seamount were performed in June–July 2003 using the remotely operated vehicle *Victor* off the R/V *L'Atalante* [Sarradin *et al.*, 2001], just 3 months after the earthquake swarm. It needs to be noted that the survey performed using *Victor* was done without knowledge that a potentially magmatic earthquake swarm had occurred at Lucky Strike. Had the earthquake information been available, a different approach to surveying the summit vent fields may have been undertaken to quantify better the evidence for or against recent magmatic activity.

[18] A high-temperature vent site east of the lava lake, last observed in 1999, now exhibited both diffuse and high-temperature venting and roughly 10 patches of new bacterial floc and/or mats ( $\sim 2 \text{ m}^2$  in area). This microbial activity was comparable in intensity (although less widespread) to the microbial bloom following the major seafloor eruption on the East Pacific Rise in 1991 [Haymon *et al.*, 1993]. Moreover, in situ observations of the Lucky Strike hydrothermal field obtained from submersible dives during July 2002 (T. Shank, personal communication, 2003) suggest an increase in diffuse venting, especially along the sides and base of the black smoker mounds, since the site was last visited in 1997. There was, however, no evidence of recent lava flows and the previously observed hydrothermal vent chimneys were intact. The evidence presented here is consistent with emplacement of a dike into the shallow crust of Lucky Strike Seamount, causing an increase in hydrothermal fluid temperatures and microbial activity, but

not necessarily resulting in an eruption of lava onto the seafloor.

## 6. Horizontal Extension

[19] Given the March 2001 earthquake swarm was the largest swarm detected at the Lucky Strike segment since modern teleseismic monitoring began, it is interesting to investigate how much of the long-term seafloor spreading rate was accommodated by the earthquake swarm. The amount of horizontal extension caused by seismicity from the Lucky Strike swarm can be estimated using a simple model of lithospheric extension along a ridge axis median valley floor developed by Solomon *et al.* [1988]. This generalized model developed for the MAR assumes extension occurs predominantly by normal faulting of the brittle lithosphere, which may not be the case for the Lucky Strike swarm since if a magma dike injection occurred, a significant amount of plate separation occurred through aseismic extension. The assumption is, however, useful for estimating the minimum amount of ridge extension that occurred during the earthquake swarm. In their model, the sum of the seismic moment  $M_o$  release rate per unit time,  $T$ , is defined as

$$\frac{\sum M_o}{T} = 2\mu Lvh/(\sin\theta \cos\theta), \quad (1)$$

where  $L$  is the segment length,  $h$  is the thickness of the brittle layer,  $v$  is the half spreading rate, and  $\mu$  is the shear modulus of ocean crust. It is assumed that all

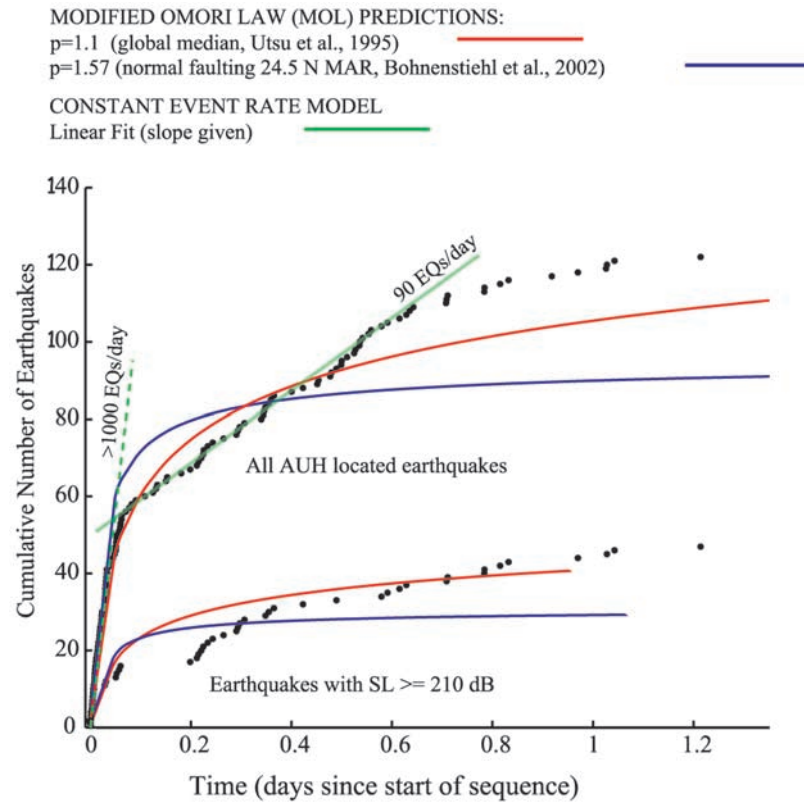


**Figure 10.** Cumulate number of Lucky Strike earthquakes shown as a function of time for both the full catalog of earthquakes located on hydrophones and the subset with source levels (SLs)  $\geq 210$  dB. Curves indicate the expected event rate for a main shock–aftershock sequence, with decay constants ( $p$  values) of 1.1 (red [Utsu et al., 1995]) and 1.57 (blue [Bohnenstiehl et al., 2002]) These event rate curves do not describe the observed distribution well, relative to previous hydrophone recorded aftershock sequences, and the event rate can be better described by a linear model (dashed green line), with an abrupt rate change near 0.05 day.

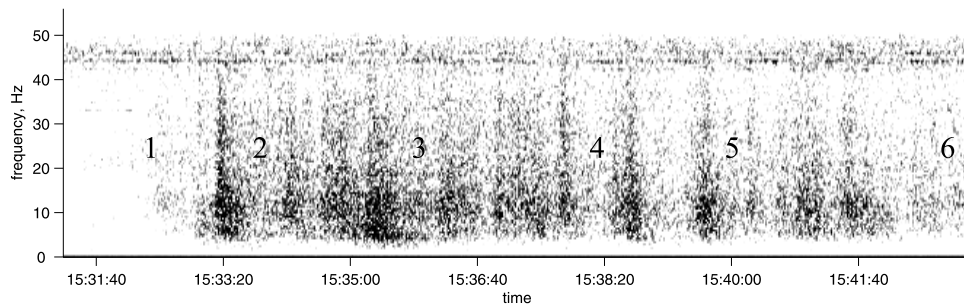
extension of the brittle layer occurs by slip on normal, planar faults that extend to depth  $h$  and dip at an inward angle  $\theta$ . Note that equation (1) is independent of the width of the valley inner floor and fault slip during an earthquake, both of which are proportional to horizontal strain and can be factored out of the equation. The total moment release from the earthquake swarm can be estimated using the relation

$$\log_{10}(M_0) = m_b + 18.52 \quad (2)$$

developed by Okal and Romanowicz [1994] for earthquakes with  $m_b \leq 4.96$  to account for saturation of the  $m_b$  scale. Summing the moments of the 33 earthquakes detected by NEIC during the Lucky Strike swarm yields a total moment of  $3.26 \times 10^{24}$  dyn cm. Next, assuming a 50 km segment length, seismic zone depth of 10 km, a fault dip of  $56^\circ$  (from the Harvard CMT solution), and a shear modulus of  $3 \times 10^{11}$  dyn  $\text{cm}^{-2}$ , then solving for half spreading rate  $v$  results in an estimate of 5.0 mm half or 10.0 mm full horizontal extension based on the seismic earthquake information. Because of the limited magnitude range of the seismic catalog ( $M_{\max} - M_c < 0.5 m_b$ ), the moment-frequency exponent ( $\beta$ ) cannot be resolved, and

the distribution cannot be extrapolated reliably to estimate the moment release of the smaller magnitude events [e.g., Molnar, 1979].

[20] A similar estimate of extension also can be made using the source levels (acoustic magnitude) of the hydrophone detected earthquakes. Figure 13 shows the regression relationship of the source level to body wave magnitudes of the Lucky Strike earthquakes. The source level of a seafloor earthquake is calculated for each receiving hydrophone by removing the effects of acoustic attenuation along the propagation path from source to receiver (spherical spreading from seafloor to sound channel; cylindrical spreading along the sound channel path) and the hydrophone instrument response from the  $T$  wave signal packet [Dziak, 2001]. Source levels are measured in decibels (dB) relative to micropascals at 1 m, and are the mean of all hydrophones that recorded the earthquake. The result is an estimate of the acoustic energy the earthquake released into the water column at the seafloor-ocean interface. Acoustic attenuation estimates (transmission loss) for propagation paths from the MAR to each hydrophone are typically  $100 \pm 10$  dB [Dziak, 2001]. Since the direct physical relationship between the seismic magnitude and source levels are not known, empirical analyses must



- (1) Ambient power = 69.8 dB, 1-30 Hz, 66.6 sec duration
- (2) Inter-earthquake power = 97.7 dB, 1-30 Hz, 17.0 sec duration
- (3) Inter-earthquake power = 99.0 dB, 1-30 Hz, 7.0 sec duration
- (4) Inter-earthquake power = 92.6 dB, 1-30 Hz, 51.1 sec duration
- (5) Inter-earthquake power = 91.9 dB, 1-30 Hz, 18.5 sec duration
- (6) Ambient power = 73.0 dB, 1-30 Hz, 27.4 sec duration

**Figure 11.** Spectrogram (dB power as a function of time) of the onset the of Lucky Strike earthquake swarm showing interearthquake energy level. This record is from the northeast hydrophone, closest station to the Lucky Strike segment. The portion of the northeast hydrophone record used here is shown in Figure 3. Numbers on the spectrogram show the location of the relative power calculations, with the frequency range and time duration of the power estimates shown in the table. The 1–30 Hz band was chosen since the hydrophone band pass filter begins at 1 Hz and the tremor energy appears present up to 30 Hz. Power level estimates show there is significant energy between earthquake signal packets (2, 3, 4, and 5) that is well above ambient noise levels (1 and 6). This interearthquake energy may be a hydroacoustic form of volcanic tremor, similar to tremor observed at subaerial volcanic systems.

be used to develop a seismic to acoustic magnitude scaling relationship (Figure 13), where the regression line follows the form

$$SL = 2.80 m_b + 201.99. \quad (3)$$

Thus, with equations (2) and (3), seismic moment release from earthquakes detected on the hydrophones can be obtained, yielding a full horizontal extension estimate of 76.1 mm. This estimate, however, may imply an uncharacteristically large moment contribution from the smaller earthquakes, suggesting that equation (3) overestimates the magnitude of some hydroacoustically detected events. In developing equation (3), only earthquakes with acoustic and seismic origin times within  $\pm 30$  s were used to ensure the events were correlated between catalogs. Thus only 19 of the 33 NEIC detected earthquakes were used to estimate equation (3). In comparison, a source level to body wave magnitude relationship of  $SL = 18.95m_b + 151.91$  was also developed based on the entire MAR hydrophone earthquake database [Dziak *et al.*, 2004]. It seems likely the scaling relationship based on the complete hydroacoustic catalog provides a more robust evaluation of the  $SL-m_b$  relationship; however, this relation underestimates the teleseismically determined magnitudes shown in Figure 13, yielding a full horizontal extension estimate of only 1.7 mm.

[21] Comparing the seismic and acoustic extension estimates to the long-term, full spreading rate of  $21 \text{ mm yr}^{-1}$  at Lucky Strike suggests the March 2001 swarm may have accommodated from 0.1 to 3.6 years (acoustic) or 0.5 year

(seismic) of seafloor spreading. These estimates are not particularly well constrained, and provide only a minimum assessment of extension since the model does not account for the aseismic component. These estimates do, however,

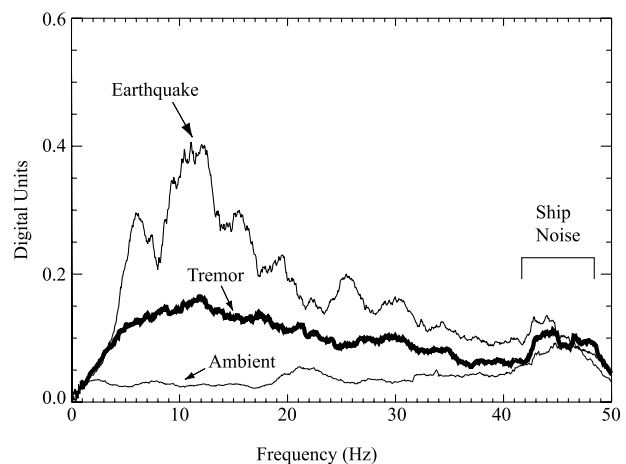


**Figure 12.** Diagram of the detailed spectra of an earthquake, volcanic tremor, and ambient noise from the northeast hydrophone during the onset of the Lucky Strike swarm. If the tremor signal is a result of magma injecting through the crust and not simply reverberation (reflection/refraction) of the earthquake signal in the water column, then it should have a different frequency content than the earthquakes. The tremor and earthquake have different dominant frequencies, although their overall bandwidth appears to be the same (ship noise dominates the  $>42$  Hz range).

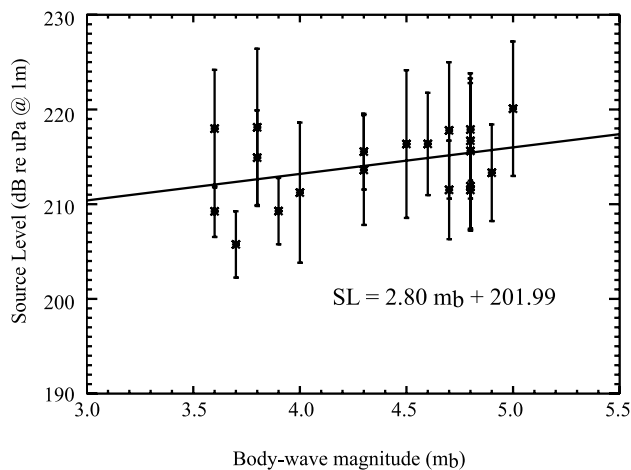


**Figure 13.** NEIC body wave magnitude ( $m_b$ ) versus acoustic source level (SL), with one standard deviation error bars, for earthquakes from the Lucky Strike swarm. Black line shows the least squares fit of these data, with the attendant SL- $m_b$  relationship.

render a baseline for comparison with future MAR seafloor spreading events.

## 7. Discussion

[22] The Lucky Strike swarm has several characteristics similar to documented plume-producing, extrusive events observed on the Juan de Fuca Ridge (JdFR). These include a vigorous earthquake swarm (>25 earthquakes per hour during the first 2 hours), continuous tremor-like energy at the swarm's onset, and no initial main shock. The time distribution and magnitudes of hydroacoustic seismicity suggests this was not a main shock-aftershock (tectonic) sequence, but fits the definition of an earthquake swarm with a magmatic component. Moreover, intrusion tremor observed at Krafla Volcano in Iceland is very similar to the tremor observed here, with a broad spectrum and dominant frequencies >3 Hz [Brandsdottir and Einarsson, 1992]. Small earthquake swarms (<100 events) at Krafla [Bjornsson, 1985] and Axial Volcano along the JdFR [Dziak and Fox, 1999] have been shown to represent intrusions of magma beneath the volcano's summit and into adjacent rift zones. Intrusion tremor and earthquakes typically stop once magma reaches the surface or the dike stops propagating.

[23] Interpretation of the risetimes (relative depths) and the relative temporal distribution of the hydrophone and seismic recorded earthquakes suggest an initial intrusion of magma into the shallow crust at the onset of the swarm, followed by segment-scale normal faulting (large magnitude earthquakes) in response to the stress perturbation induced by the magmatic intrusion. In addition, the earthquakes were apparently the most shallow at and near Lucky Strike Seamount, then deepened through time and at the distal ends of the segment. This pattern is consistent with the risetime distributions observed during a dike emplacement/seafloor eruption episode at Axial Volcano, a seamount located in the center of a ridge segment [Dziak and Fox, 1999]. During this magmatic event, earthquakes were shallow (short risetimes) during the onset of the swarm at the

summit of the seamount, which were also the location and time of the observed seafloor eruption [Fox, 1999; Baker et al., 1999]. As the magma dike propagated down rift away from the source magma body (the summit of Axial), the earthquakes also migrated down rift and progressively deepened, apparently tracking the injection of the dike deeper into the crust at the distal end of the segment [Dziak and Fox, 1999].

[24] There are, however, notable elements missing when compared to previously documented mid-ocean ridge eruption episodes. On intermediate rate ridge segments, for example, typically eruptions produce earthquake swarms with durations from one to several weeks, while the Lucky Strike swarm lasted only 29 hours. Documented eruption events also have exhibited significant (>10 km) migration of earthquakes along strike of the ridge segment [e.g., Dziak et al., 1995]. This earthquake migration is caused by the lateral propagation of a magma dike into the shallow crust of the rift zone. The Lucky Strike swarm showed no obvious earthquake migration, rather the seismicity appeared to occur almost simultaneously along the entire ~50 km length of the segment, both at the summit of Lucky Strike Seamount and northward (Figure 6). In addition, previously documented mid-ocean ridge eruptions generally produce an abundance of seafloor and water column observations confirming magmatic activity, although the 2001 Middle Valley (JdFR) and Jackson segment (Gorda Ridge) seafloor spreading events produced no clear water column signatures [Davis et al., 2004; Fox et al., 2001b]. In situ observations of the Lucky Strike hydrothermal field obtained from submersible dives within a year of the earthquake swarm, and without prior knowledge of the 2001 swarm, indicate significant increases in microbial activity and diffuse venting. However, no evidence of recent lava flows has yet been observed, and all preexisting hydrothermal vents appear to still be intact.

[25] In comparison to other observed seafloor spreading and extension episodes, the Lucky Strike event was much smaller than previous estimates. The 1979 eruption of Krafla Volcano exhibited 8 m of extension and accommodated several hundreds of years of spreading along the slow spreading MAR [Bjornsson, 1985]. The eruption of Axial Volcano along the intermediate spreading Juan de Fuca Ridge (JdFR) in 1998 resulted in 248 mm of horizontal extension, accommodating ~4.5 years of seafloor spreading, based on acoustic estimates [Dziak and Fox, 1999]. Seismic and hydrologic estimates suggest a magma injection event at the Endeavour segment of the JdFR in 1999 caused ~120 mm of total extension at the ridge axis [Davis et al., 2001]. Magmatic activity at Axial and Krafla volcanoes provide particularly useful analogies to Lucky Strike because they are both associated with the interaction of a mantle hot spot and a mid-ocean ridge.

[26] We interpret the March 2001 earthquake swarm at Lucky Strike as a magma/dike emplacement episode that may have occurred without an eruption of lava on to the seafloor, similar to magma replenishment events observed at volcanoes in Iceland [Bjornsson et al., 1977; Tryggvason, 1994]. Studies constraining the ages of MAR axial valley lavas indicate the upper crust of a slow spreading ridge segment dominated by discrete volcanoes may be constructed by dispersed, isolated eruptions occurring intermit-

tently over many tens of thousands of years [Sturm *et al.*, 2000]. Thus the Lucky Strike swarm may have been an example of one of these discrete, upper crust constructional events. Even without a seafloor eruption, however, a shallow dike emplacement event would in all likelihood have produced a measurable increase in the fluid temperatures, flux rates, and microbial activity at preexisting hydrothermal systems. The earthquake activity itself, in addition to magmatic influences, can cause significant changes (via ground motion) to vent fluid temperatures and flux rates [Dziak and Johnson, 2002] which can have a profound effect on the populations of macro-organisms and micro-organisms inhabiting the hydrothermal vent sites [Summit and Baross, 2001; Cowen *et al.*, 2004]. Unfortunately, it would be difficult to link perturbations currently observed at the hydrothermal sites to the 2001 earthquake swarm now that it is more than 3 years after the event occurred.

## 8. Summary

[27] The Lucky Strike swarm was one of the most significant earthquake swarms to occur along the northern MAR in 20+ years of monitoring. Small, relatively short duration earthquake swarms have been observed 5–10 years prior to large eruptions at Axial and Krafla Volcanoes, and it could be the Lucky Strike swarm is a precursor to increased seismic and volcanic activity at the Lucky Strike Seamount and segment. It remains to be seen, however, how this magmatic episode fits into the overall volcanic cycle of Lucky Strike and the northern MAR as a whole. The exact nature of volcanic activity along the slow spreading MAR has been the subject of much speculation since it is not known how frequently magmatic events occur or whether there are spatial patterns to these events. Our results suggest that one form of volcanism along the Mid Atlantic Ridge may be due to highly focused pockets of magma that produce sporadic intrusions into shallow ocean crust, creating long-lived, discrete volcanic structures and leading to recharge of preexisting seafloor hydrothermal vents and ecosystems.

[28] Recently, the Monitoring of the MAR (MOMAR) Project was formed to promote international cooperation to establish long-term multidisciplinary monitoring near the Azores region. The Lucky Strike area was selected at the first MOMAR workshop as the most appropriate site to begin vent and segment-scale monitoring experiments. The March 2001 Lucky Strike earthquake swarm provides strong evidence that the Lucky Strike area is an excellent candidate for monitoring magmatic/volcanic activity, seafloor deformation, and hydrothermal vent processes along the MAR.

[29] **Acknowledgments.** The authors wish to thank J. Haxel and M. Fowler for their data analysis and at sea support, T.-K. Lau for developing the analysis software, and E. Klein, J. Cowen, and D. Blackman for very helpful reviews. This study was made possible through the support of the U.S. National Science Foundation (grants OCE-9811575, OCE-0137164, and OCE-0201692) and the NOAA Vents Program. This paper is NOAA-PMEL contribution 2681.

## References

Baker, E. T., G. J. Massoth, and R. A. Feely (1987), Cataclysmic hydrothermal venting on the Juan de Fuca Ridge, *Nature*, *329*, 149–151.

- Baker, E. T., G. J. Massoth, R. A. Feely, R. W. Embley, R. E. Thomson, and B. J. Burd (1995), Hydrothermal event plumes from the CoAxial seafloor eruption site, Juan de Fuca Ridge, *Geophys. Res. Lett.*, *22*, 147–150.
- Baker, E. T., C. G. Fox, and J. P. Cowen (1999), In situ observations of the onset of hydrothermal discharge during the 1998 submarine eruption of Axial Volcano, Juan de Fuca Ridge, *Geophys. Res. Lett.*, *26*(23), 3445–3448.
- Ballard, R. D., and T. H. van Andel (1977), Morphology and tectonics of the inner rift valley at lat 36°50'N on the Mid-Atlantic Ridge, *Geol. Soc. Am. Bull.*, *88*, 507–530.
- Bevington, P. R., and D. K. Robinson (1992), *Data Reduction and Error Analysis for the Physical Sciences*, McGraw-Hill, New York.
- Bjornsson, A. (1985), Dynamics of crustal rifting in Iceland, *J. Geophys. Res.*, *90*, 10,151–10,162.
- Bjornsson, A., K. Saemundsson, P. Einarsson, E. Tryggvason, and K. Gronvold (1977), Current rifting episode in north Iceland, *Nature*, *266*, 318–323.
- Blackman, D. K., C. E. Nishimura, and J. A. Ocrutt (2000), Seismoacoustic recordings of a spreading episode on the Mohns Ridge, *J. Geophys. Res.*, *105*, 10,961–10,973.
- Bohnenstiehl, D. R., and M. Tolstoy (2003), Comparison of teleseismic and hydroacoustic-derived earthquake locations along the north-central Mid-Atlantic Ridge and equatorial East Pacific Rise, *Seismol. Res. Lett.*, *74*, 791–802.
- Bohnenstiehl, D. R., M. Tolstoy, D. K. Smith, D. R. Bohnenstiehl, C. G. Fox, and R. P. Dziak (2002), Aftershocks sequences in the mid-ocean ridge environment: An analysis using hydroacoustic data, *Tectonophysics*, *354*, 49–70.
- Bohnenstiehl, D. R., M. Tolstoy, D. K. Smith, C. G. Fox, and R. P. Dziak (2003), Time clustering behavior of earthquakes along the Mid-Atlantic Ridge 15°–35°N: Observations from hydroacoustic monitoring, *Phys. Earth Planet. Inter.*, *138*(2), 147–161.
- Brandstottir, B., and P. Einarsson (1992), Volcanic tremor and low-frequency earthquakes in Iceland, in *IAVCEI Proceedings in Volcanology*, edited by P. Gasparini, R. Scarpa, and K. Aki, pp. 212–222, Springer-Verlag, New York.
- Chouet, B. A. (1992), A seismic model for the source of long-period events and harmonic tremor, in *Volcanic Seismology*, edited by P. Gasparini, R. Scarpa, and K. Aki, pp. 133–156, Springer-Verlag, New York.
- Corliss, J. B., et al. (1979), Submarine thermal springs on the Galapagos Rift, *Science*, *203*, 1073–1083.
- Cowen, J. P., E. T. Baker, and R. W. Embley (2004), Detection of and response to mid-ocean ridge magmatic events: Implications for the subsurface biosphere, in *The Seafloor Biosphere at Mid-Ocean Ridges*, *Geophys. Monogr. Ser.*, vol. 144, edited by W. S. D. Wilcock et al., pp. 227–243, AGU, Washington, D. C.
- Davis, E. E., K. Wang, R. E. Thomson, K. Becker, and J. F. Cassidy (2001), An episode of seafloor spreading and associated plate deformation inferred from crustal fluid pressure transients, *J. Geophys. Res.*, *106*, 21,953–21,963.
- Davis, E. E., K. Becker, R. Dziak, J. Cassidy, K. Wang, and M. Lilley (2004), A hydrologic response to a seafloor spreading episode on the Juan de Fuca Ridge, *Nature*, *430*, 335–338.
- Davis, T. M., K. A. Countryman, and M. J. Carron (1986), Tailored acoustic products utilizing the NAVOCEANO GDEM (a generalized digital environmental model), paper presented at 36th Naval Symposium on Underwater Acoustics, Naval Ocean Syst. Cent., San Diego, Calif.
- Detrick, R. S., H. D. Needham, and V. Renard (1995), Gravity anomalies and crustal thickness variations along the Mid-Atlantic Ridge between 33°N and 40°N, *J. Geophys. Res.*, *100*, 3767–3787.
- Dziak, R. P. (2001), Empirical relationship of *T*-wave energy and fault parameters of northeast Pacific Ocean earthquakes, *Geophys. Res. Lett.*, *28*, 2537–2540.
- Dziak, R. P., and C. G. Fox (1999), Long-term seismicity and ground deformation at Axial Volcano, Juan de Fuca Ridge, *Geophys. Res. Lett.*, *26*, 3641–3644.
- Dziak, R. P., and H. P. Johnson (2002), Stirring the oceanic incubator, *Science*, *296*, 1406–1407.
- Dziak, R. P., C. G. Fox, and A. E. Schreiner (1995), The June–July 1993 seismo-acoustic event at CoAxial segment, Juan de Fuca Ridge: Evidence for a lateral dike injection, *Geophys. Res. Lett.*, *22*, 135–138.
- Dziak, R. P., C. G. Fox, H. Matsumoto, and A. E. Schreiner (1997), The April 1992 Cape Mendocino earthquake sequence: Seismo-acoustic analysis utilizing fixed hydrophone arrays, *Mar. Geophys. Res.*, *19*, 137–162.
- Dziak, R. P., D. R. Bohnenstiehl, H. Matsumoto, C. G. Fox, D. K. Smith, M. Tolstoy, T.-K. Lau, J. H. Haxel, and M. J. Fowler (2004), *P*- and *T*-wave detection thresholds, *P<sub>n</sub>* velocity estimate, and detection of lower mantle and core *P*-waves on ocean sound-channel hydrophones at the Mid-Atlantic Ridge, *Bull. Seismol. Soc. Am.*, *94*, 665–677.

- East Pacific Rise Study Group (1981), Crustal processes of the mid-ocean ridge (in solid earth), *Science*, *213*, 31–40.
- Einarsson, P. (1991), Earthquakes and present-day tectonism in Iceland, *Tectonophysics*, *189*, 261–279.
- Embley, R. W., W. W. Chadwick Jr., I. R. Jonasson, D. A. Butterfield, and E. T. Baker (1995), Initial results of the rapid response to the 1993 CoAxial event: Relationships between hydrothermal and volcanic processes, *Geophys. Res. Lett.*, *22*, 143–146.
- Embley, R. W., W. W. Chadwick, D. Clague, and D. Stakes (1999), 1998 eruption of Axial Volcano: Multibeam anomalies and sea-floor observations, *Geophys. Res. Lett.*, *26*, 3425–3428.
- Escartin, J., M. Cannat, G. Poulouquen, A. Rabain, and J. Lin (2001), Crustal thickness of V-shaped ridges south of the Azores: Interaction of the Mid-Atlantic Ridge (36°–39°N) and the Azores hotspot, *J. Geophys. Res.*, *106*, 21,719–21,736.
- Escartin, J., D. K. Smith, and M. Cannat (2003), Parallel bands of seismicity at the Mid-Atlantic Ridge, 12–14°N, *Geophys. Res. Lett.*, *30*(12), 1620, doi:10.1029/2003GL017226.
- Fox, C. G. (1999), In situ ground deformation measurements from the summit of Axial Volcano during the 1998 volcanic episode, *Geophys. Res. Lett.*, *26*, 3437–3440.
- Fox, C. G., R. P. Dziak, H. Matsumoto, and A. E. Schreiner (1994), Potential for monitoring low-level seismicity on the Juan de Fuca Ridge using military hydrophone arrays, *Mar. Technol. Soc. J.*, *27*, 22–30.
- Fox, C. G., W. E. Radford, R. P. Dziak, T.-K. Lau, H. Matsumoto, and A. E. Schreiner (1995), Acoustic detection of a seafloor spreading Episode on the Juan de Fuca Ridge using military hydrophone arrays, *Geophys. Res. Lett.*, *22*, 131–134.
- Fox, C. G., H. Matsumoto, and T. K. A. Lau (2001a), Monitoring Pacific Ocean seismicity from an autonomous hydrophone array, *J. Geophys. Res.*, *106*, 4183–4206.
- Fox, C. G., J. P. Cowen, R. P. Dziak, E. T. Baker, R. W. Embley, W. W. Chadwick, J. E. Lupton, J. A. Resing, and S. R. Hammond (2001b), Detection and response to a seafloor spreading episode on the central Gorda Ridge, April 2001, *Eos Trans. AGU*, *82*(47), Fall Meet. Suppl., Abstract S22C-05.
- Haymon, R. M., et al. (1993), Hydrothermal vent distribution along the East Pacific Rise crest and its relationship to magmatic and tectonic processes on fast-spreading mid-ocean ridges, *Earth Planet Sci Lett.*, *119*, 85–101.
- Holden, J. F., M. Summit, and J. A. Baross (1998), Thermophilic and hyperthermophilic microorganisms in 3–30°C hydrothermal fluids following a deep-sea volcanic eruption, *FEMS Microbiol. Ecol.*, *25*, 33–41.
- Humphris, S. E., D. J. Fornari, D. S. Scheirer, C. R. German, and L. M. Parson (2002), Geotectonic setting of hydrothermal activity on the summit of Lucky Strike Seamount (37°17'N, Mid-Atlantic Ridge), *Geochem. Geophys. Geosyst.*, *3*, 1049, doi:10.1029/2001GC000284.
- Johnson, R. H., R. A. Norris, and F. K. Duennebier (1968), Abyssally generated T-phases, in *The Crust and Upper Mantle of the Pacific Area*, *Geophys. Monogr. Ser.*, vol. 12, edited by L. Knopoff, C. L. Drake, and P. J. Hart, pp. 70–78, AGU, Washington, D. C.
- Juniper, S. K., P. Martineu, J. Sarrazin, and Y. Gelin (1995), Microbial-mineral floc associated with nascent hydrothermal activity on CoAxial segment, Juan de Fuca Ridge, *Geophys. Res. Lett.*, *22*, 179–183.
- Mogi, K. (1963), Some discussions on aftershocks, foreshocks and earthquake swarms—The fracture of a semi-infinite body caused by an inner stress origin and its relation to the earthquake phenomena, *Bull. Earthquake Res. Inst. Univ. Tokyo*, *41*, 615–658.
- Molnar, P. (1979), Earthquake recurrence intervals and plate tectonics, *Bull. Seismol. Soc. Am.*, *69*, 115–133.
- Okal, E. A., and B. A. Romanowicz (1994), On the variation of *b*-values with earthquake size, *Phys. Earth. Planet. Inter.*, *87*, 55–76.
- Sarradin, P. M., et al. (2001), ATOS cruise R/V *L'Atalante*, ROV *Victor*, June 22nd–July 21st 2001, *InterRidge News*, *10*, 18–20.
- Scheirer, D. S., D. J. Fornari, S. E. Humphris, and S. Lerner (2000), High-resolution seafloor mapping using the DSL-120 sonar system: Quantitative assessment of sidescan and phase-bathymetry data from the Lucky Strike segment of the Mid-Atlantic Ridge, *Mar. Geophys. Res.*, *21*, 121–142.
- Schreiner, A. E., C. G. Fox, and R. P. Dziak (1995), Spectra and magnitudes of T-waves from the 1993 earthquake swarm on the Juan de Fuca Ridge, *Geophys. Res. Lett.*, *22*, 139–142.
- Slack, P. D., C. G. Fox, and R. P. Dziak (1999), P wave detection thresholds, Pn velocity estimates, and T wave location uncertainty from oceanic hydrophone arrays, *J. Geophys. Res.*, *104*, 13,061–13,072.
- Smith, D. K., and J. R. Cann (1993), Building the crust at the Mid-Atlantic Ridge, *Nature*, *365*, 707–715.
- Smith, D. K., M. Tolstoy, C. G. Fox, D. R. Bohnenstiehl, H. Matsumoto, and M. J. Fowler (2002), Hydroacoustic monitoring of seismicity at the slow-spreading Mid-Atlantic Ridge, *Geophys. Res. Lett.*, *29*(11), 1518, doi:10.1029/2001GL013912.
- Smith, D. K., J. Escartin, M. Cannat, M. Tolstoy, C. G. Fox, D. R. Bohnenstiehl, and S. Bazin (2003), Spatial and temporal distribution of seismicity along the northern Mid-Atlantic Ridge (15°–35°N), *J. Geophys. Res.*, *108*(B3), 2167, doi:10.1029/2002JB001964.
- Solomon, S. C., P. Y. Huang, and L. Menke (1988), The seismic moment budget of slowly spreading ridges, *Nature*, *334*, 58–60.
- Spies, F. N., et al. (1980), East Pacific Rise: Hot springs and geophysical experiments, *Science*, *207*, 1421–1433.
- Sturm, M., S. Goldstein, E. M. Klein, J. A. Karson, and M. T. Murrell (2000), Uranium-series age constraints on lavas from the axial valley of the Mid-Atlantic Ridge, MARK area, *Earth Planet. Sci. Lett.*, *181*, 61–70.
- Summit, M., and J. A. Baross (2001), A novel microbial habitat in the mid-ocean ridge sub-seafloor, *Proc. Natl. Acad. Sci. U.S.A.*, *98*, 2158–2163.
- Sykes, L. R. (1970), Earthquake swarms and sea-floor spreading, *J. Geophys. Res.*, *75*, 6598–6611.
- Tolstoy, M., D. R. Bohnenstiehl, M. H. Edwards, and G. J. Kurras (2001), Seismic character of volcanic activity at the slow-spreading Gakkel Ridge, *Geology*, *29*, 1139–1142.
- Tryggvason, E. (1994), Surface deformation at the Krafla Volcano, north Iceland 1982–1992, *Bull. Volcanol.*, *56*, 98–107.
- Utsu, T., Y. Ogata, and R. S. Matsuura (1995), The centenary of the Omori formula for a decay law of aftershock activity, *J. Phys. Earth*, *43*(1), 1–33.
- Yang, Y., and D. W. Forsyth (2003), Improving epicentral and magnitude estimation of earthquakes from T-phases by considering the excitation function, *Bull. Seismol. Soc. Am.*, *93*, 2106–2122.

D. R. Bohnenstiehl, Lamont-Doherty Earth Observatory, Box 1000, 61 Route 9W, Palisades, NY 10964, USA.

D. Desbruyeres, Departement Environnement Profond, Centre de Brest de l'IFREMER, BP 70, F-29280 Plouzane Cedex, France.

R. P. Dziak and H. Matsumoto, OSU/NOAA, Hatfield Marine Science Center, 2115 SE OSU Drive, Newport, OR 97365, USA. (robert.p.dziak@noaa.gov)

D. J. Fornari and D. K. Smith, Woods Hole Oceanographic Institution, MS 22, Woods Hole, MA 02543, USA.

C. G. Fox, National Geophysical Data Center, 325 Broadway, Boulder, CO 80305-3328, USA.

M. Tolstoy, Oceanography 108-E, Lamont-Doherty Earth Observatory, 61 Route 9W, Palisades, NY 10964-8000, USA.